**Article:**
Menchicchi, B, Savvaidou, E, Thöle, C et al. (2 more authors) (2019)
Low-Molecular-Weight Dextran Sulfate Nanocapsules Inhibit the Adhesion of Helicobacter pylori to Gastric Cells. ACS Applied Bio Materials, 2 (11). pp. 4777-4789. ISSN 2576-6422

https://doi.org/10.1021/acsabm.9b00523

# Low-molecular-weight dextran sulfate nanocapsules inhibit the adhesion of Helicobacter pylori to gastric cells

Bianca Menchicchi[a,b], Eleni Savvaidou[a], Christian Thöle[c] Andreas Hensel[c*],

Francisco M. Goycoolea[a,d*]

[a)] University of Münster, Institute of Plant Biology and Biotechnology (IBBP), Schlossplatz 8, D-48143 Münster, Germany

[b)]Department of Medicine 1, University of Erlangen-Nüremberg, D-91054 Erlangen, Germany

[c)]University of Münster, Institute for Pharmaceutical Biology and Phytochemistry (IPBP), Correnstrasse 48, D-48149 Münster, Germany

[d)]School of Food Science and Nutrition, University of Leeds, Leeds LS2 9JT, Leeds, United Kingdom

* Authors for correspondence:

Francisco M. Goycoolea (F.M.Goycoolea@leeds.ac.uk)

Andreas Hensel (ahensel@uni-muenster.de)

**Abstract**

The Gram-negative bacterium Helicobacter pylori is the most common bacterial pathogen in humans, infecting 24–79% of the population at any time. Standard eradication protocols involve multi-target therapy including combinations of antibiotics, which has promoted the emergence of resistant strains. To address this challenge, we prepared antibiotic-free colloidal nanoparticles designed to interfere with the adhesion mechanisms of H. pylori and thus prevent both the onset and recurrence of infection. Our colloidal particles comprised a nanocapsule (NC) formulation based on an oil-core nanoemulsion co-stabilized with lysozyme and lecithin, coated with negatively-charged low-molecular-weight (DexS40-NC) or high-molecular-weight (DexS500-NC) dextran sulfate, or positively-charged chitosan ($CS_{HMC+30}$-NC). The oil core of all NC formulations was also loaded with curcumin, a model lipophilic drug with well-documented documented anti-inflammatory and anti-tumor activities. Our proof-of-principle experiments showed that the DexS40-NC formulation inhibited the adhesion of H. pylori to AGS stomach cells in a dose-dependent manner. DexS40-NC achieved more potent inhibition than DexS500-NC or uncoated control nanoemulsions, whereas the effect of $CS_{HMC+30}$-NC was not clearcut given the ability of this formulation to aggregate bacteria. DexS40-NC, unlike DexS500-NC, showed no cytotoxic effects against AGS, Caco-2, or MDCK cell lines. DexS40-NC is, therefore, a promising candidate for further development as an alternative or complementary therapy against H. pylori infections.

**Keywords:** bacterial anti-adhesion, antibiotic resistance, chitosan, nanoemulsion, AGS cells

Conflict of interest: A patent has been filed related to the work described in this article.

## Introduction

Helicobacter pylori is a Gram-negative bacterial pathogen carried by 4.4 billion people worldwide [1]. The prevalence of H. pylori is highest in Africa (79.1%), Latin America and the Caribbean (63.4%), and Asia (54.7%), and lowest in North America (37.1%), Western Europe (34.3%) and Oceania (24.4%). Although 80% of infections are asymptomatic, the pathogen causes chronic gastritis and gastric ulcers, and is associated with an increased risk of gastric cancer [2, 3]. Unlike other bacteria, H. pylori thrives in the acidic stomach by creating a favorable environment in the mucus layer, facilitating the infection of epithelial cells [4]. H. pylori infections can be eradicated by multi-target therapy using combinations of antibiotics, but the spread of antibiotic resistance has led to the development of hybrid quadruple therapies based on proton pump inhibitors, bismuth and combinations of antibiotics such as furazolidone, tetracycline, metronidazole and amoxicillin, with high eradication rates [5]. Even so, the short residence time and limited efficacy of these drugs under the mucus layer often lead to recurrent infections, promoting the emergence of resistant H. pylori strains [6]. Alternative therapeutic approaches for the eradication of this pathogen are therefore urgently required.

One strategy to address this challenge is the development of formulations that persist in the mucus layer, as shown for various liposomes and polymer-based nanoparticles [7-9]. Proteins and polysaccharides are preferred materials due to their biocompatibility and mucoadhesive properties [10]. High-molecular-weight polysaccharides interact more strongly with mucin than oligosaccharides because the polymer backbone is flexible and features more entanglement points [11]. Furthermore, charged polysaccharides such as dextran sulfate are better than neutral ones such as dextran because binding to the mucin glycoprotein is improved by electrostatic interactions [11]. Certain polysaccharides can also directly interfere with interactions between H. pylori adhesins and the gastric mucosa [12], such as those extracted from okra (Abelmoschus esculentus) [13, 14], ginseng (Panax ginseng) [15] and aloe vera (Aloe vera L. var. chinensis) [16] as well as sulfated exopolysaccharides from microalgae [17] and brown seaweeds such as Cladosiphon okamuranu [18, 19] and Fucus vesiculosus [20], both of which produce fucoidan. Dextran sulfate was shown to prevent the adhesion of H. pylori to immobilized mucin but not to a human gastric cell line. However, dextran sulfate pretreatment can inhibit the adhesion of H. pylori to heparan sulfate [21] and the urease-mediated adhesion of H. pylori to MKN45 cells under acidic conditions [22].

Thus far, there has been no attempt to explore the anti-adhesive effect of nanoparticles containing mucoadhesive dextran sulfate components. Accordingly, we prepared nanocapsule (NC) formulations featuring oil cores co-stabilized with lecithin and lysozyme (Lyz) and loaded with

curcumin as a model lipophilic drug with well-documented biological activities [23]. We evaluated the performance of formulations coated with one of two forms dextran sulfate (negative charge) differing in molecular weight, another formulation coated with chitosan (positive charge), and an uncoated control nanoemulsion (NE) with a negative charge. We characterized the biophysical properties of each formulation and compared them in terms of their interaction with pancreatic phospholipase ($PLA_2$), their cytotoxicity towards three cell lines (human Caco-2 and AGS gastrointestinal carcinoma lines and the canine kidney cell line MDCK) and their ability to block the adhesion of H. pylori to AGS cells. An optimal formulation with mucin-binding activity and anti-adhesive effects would provide a valuable new approach for the development of antibiotic-free therapies for the eradication of H. pylori.

## Materials and methods

### Materials

Soybean lecithin (Epikuron 145v) was purchased from Cargill (Hamburg, Germany) and Mygliol 812 N was purchased from Sasol (Witten, Germany). The low-molecular-weight (DexS40) and high-molecular-weight (DexS500) sodium salts of dextran sulfate from Leuconostoc spp. were purchased from Merck KGaA (Darmstadt, Germany). DexS40 has the following properties: Mw 49,000; $[\eta]_{H2O\ pH\ 4.5}$ = 53 mL/g; $[\eta]_{0.1M\ NaCl\ pH\ 4.5}$ = 14 mL/g. DexS500 has the following properties: Mw 632,000; $[\eta]_{H2O\ pH\ 4.5}$ = 828 mL/g; $[\eta]_{0.1M\ NaCl\ pH\ 4.5}$ = 76 mL/g. Lyz from chicken egg white (dialyzed, lyophilized powder ~100,000 units/mg protein), curcumin, $PLA_2$ from porcine pancreas (ammonium sulfate suspension, ≥600 units/mg protein), porcine stomach mucin (type III, bound sialic acid 0.5–1.5%, partially-purified powder [11,12]), fluorescein-5-isothiocyanate isomer I (FITC), bovine serum albumin (BSA) and RPMI-1640 were also purchased from Merck KGaA. Pharmaceutical-grade chitosan $CS_{HMC+30}$ (DA 32.3%, Mw 17,600) was purchased from $HMC^+$ (Halle/Saale, Germany). Fetal bovine serum, 100x penicillin-streptomycin solution and 100x L-glutamine were obtained from PAA Laboratories (Pasching, Austria). Tryptic soy agar (TSA) and Tween-20 were purchased from Merck KGaA. Sheep blood (defibrinated, sterile, without additives for microbiological purposes) was obtained from Oxoid (Wesel, Germany).

### Solutions

Dextran sulfate, Lyz and $CS_{HMC+30}$ solutions were prepared in MilliQ water by gentle magnetic stirring overnight. For the total dissolution of $CS_{HMC+30}$, a 5% stoichiometric excess of HCl was

added. Each solution was filtered through a 5-µm pore membrane. Curcumin was dissolved in absolute ethanol at a maximum concentration of 1.5 mg/mL. Purified porcine stomach mucin was dissolved in PBS (pH 6.8) at a concentration of 1 mg/mL.

## Preparation of nanocapsules

NCs comprising a lysozyme nanoemulsion (NE-Lyz) coated with DexS40 or DexS500 were prepared by solvent displacement [24] with modifications. Briefly, an organic phase was prepared by dissolving 40 mg of lecithin in 0.5 mL ethanol and then adding 150 µL Mygliol and 9 mL acetone. This was poured into 20 mL water containing 0.75 mg/mL Lyz and the pH was adjusted to 4.5. The NE-Lyz dispersion (primary emulsion) was divided into six 5-mL aliquots and 1 mL DexS40 or DexS500 (concentrations of 0.01, 0.1, 0.5, 1 or 2 mg/mL) was added to each aliquot by magnetic stirring at 1500 rpm. The organic solvent and part of the water were evaporated to 30% of the initial volume by exposure to a pressure gradient (5 min at 150 mbar, 5 min at 80 mbar and 10 min at 40 mbar) at 37 °C in a Büchi Rotavapor fitted with an automatic pressure controller. For all subsequent experiments, higher-volume batches were prepared by following the same protocol but adding 3 mL of dextran sulfate (1 mg/mL) to 15 mL of NE-Lyz and doubling the exposure time at each pressure during evaporation. NCs coated with $CS_{HMC+30}$ were prepared according to the same protocol, but adding 3 mL of a chitosan solution (0.1 mg/mL) instead of dextran sulfate. NEs were prepared as above but excluding Lyz from the aqueous phase and adding 3 mL of pure water. Curcumin-loaded NCs (cc-DexS40-NC, cc-DexS500-NC, and cc-$CS_{HMC+30}$-NC) and uncoated control nanoemulsions (cc-NE) were prepared as above but the lecithin was dissolved in 4.072 mM curcumin in ethanol. The final concentration of curcumin in each NC formulation was 169 µM. When necessary, the NC and NE formulations were isolated by centrifuging 1 mL (25,000× g, 60 min, 15 °C) in a Mikro 220R device (Hettich, Bäch, Germany) to produce a creamy top layer containing the NCs or NEs. This phase was carefully isolated with a syringe and resuspended in water.

## Characterization of nanocapsules

The Z-average hydrodynamic diameter (size distribution) of 200-fold diluted NCs was measured in water by dynamic light scattering with non-invasive back scattering (DLS-NIBS) at an angle of 173°, and the effect of the coating on the surface charge was determined by measuring the ζ-potential by mixed-laser Doppler electrophoresis and phase analysis light scattering (M3-PALS). Both measurements were acquired using a Malvern Zetasizer NanoZS (Malvern Instruments, Malvern, UK) at 25 °C. The morphology of the NE, DexS40-NC and DexS500-NC formulations (diluted 10-fold in 2% phosphotungstic acid and fixed on a carbon-coated copper grid) was determined by

transmission electron microscopy (TEM) using a Philips (Copenhagen, Denmark) CM100 instrument.

Electrokinetic properties as a function of pH

The ζ-potential of NCs in the pH range 1.2 ± 0.5 to 11.0 ± 0.5 was measured as described above, following the dilution of 10 µL of cc-DexS40-NC, cc-DexS500-NC, cc-HMC$^{+}$30-NC or cc-NE in 3 mL water and the addition of 1 M HCl or 1 M NaOH as required to reach the target pH. The Z-average diameter was also measured over time.

Efficiency of curcumin encapsulation

The efficiency of curcumin encapsulation (percentage value) was determined by centrifuging 1 mL of each NC formulation (25,000× g, 60 min, 15 °C) in a Mikro 220R device to produce a creamy top layer containing NCs, a clear subnatant containing excess components in solution, and a pellet containing excess components as complexes. The three phases were separated and the NCs and pellets were re-diluted to 1 mL in water. We then mixed 25 µL of each phase with 475 µL ethanol and centrifuged the mixture (2200× g, 5 min, room temperature) in a microfuge to precipitate the polymer, protein and lecithin residues. The quantity of curcumin in the supernatant was determined by spectrophotometry at λ = 426 nm based on a curcumin in ethanol calibration curve. The distribution of curcumin in the three phases was calculated as a percentage of the total concentration.

Stability in water and physiologically-relevant media

The stability of NCs in various physiologically-relevant media was investigated by diluting each formulation 200-fold in (a) water, (b) 0.2% NaCl, 0.7% (v/v) HCl pH 1.2 (simulated gastric fluid ($SGF_{sp}$) according to USP XXVIIII), (c) mucin (1 mg/mL) in PBS pH 6.8, (d) PBS pH 6.8, or (e) RPMI-1640 medium supplemented with 10% (v/v) fetal bovine serum, 1% (v/v) penicillin-streptomycin and 1% (v/v) L-glutamine pH 7.4, and incubating at 37°C with continuous shaking. The Z-average diameter was determined by DLS-NIBS as above after 0, 4 and 24 h.

Interaction with porcine pancreatic $PLA_2$

The interaction of NCs with porcine pancreatic $PLA_2$ was monitored by turbidimetry and by measuring the Z-average diameter before and after treatment. We mixed 10 µL $PLA_2$ ammonium sulfate suspension with 1 mL 10 mM Tris/2 mM $CaCl_2$ (pH 8), diluted the mixture two-fold by making up to 2 mL with water, and added 50 µL of the NC formulation. We then transferred 205 µL of the mixture to each well of a 96-well microtiter plate and incubated for 5 min at 37 °C in a Safire

A-5082 microplate reader (Tecan Group, Männedorf, Switzerland). We added 50 µL $PLA_2$ in reaction buffer, shook the plate for 5 s and read the absorbance at 520 nm for 100 consecutive cycles at 37 °C. Controls consisted of 205 µL of the NC solution mixed with 50 µL reaction buffer without $PLA_2$. Absorbance values were calculated relative to time 0. The Z-average size distribution was also measured, as described above.

## Cell and bacterial culture

AGS cells (adherent human stomach adenocarcinoma epithelial cell line ATCC CRL 1739) were kindly provided by Prof. Dr. med. Winfried Beil, Medizinische Hochschule, Hannover, Germany. Cells were cultured in 75-$cm^2$ culture flasks containing RPMI-1640 medium supplemented with 10% (v/v) fetal bovine serum, 1% (v/v) penicillin-streptomycin and 1% (v/v) L-glutamine at 37 °C in a 5% $CO_2$ atmosphere. Cell passages from 30 to 45 were used for all experiments. Caco-2 cells derived from heterogeneous human epithelial colorectal adenocarcinoma cells were grown in minimal essential medium (MEM) with Earle's salts supplemented with 10% (v/v) fetal bovine serum, 1% (v/v) penicillin/streptomycin, 1% (v/v) L-glutamine and 1% (v/v) non-essential amino acids. Cell passages from 35 to 47 were used for all experiments. Madin-Darby canine kidney (MDCK-C7) cells were grown in MEM with Earle's salts supplemented with 10% (v/v) fetal bovine serum, 1% (v/v) penicillin/streptomycin and 1% (v/v) L-glutamine. Cell passages from 22 to 34 were used for all experiments. H. pylori ATCC 700824 (strain J99) was grown on TSA plates enriched with 5% defibrinated sheep blood as previously described [25].

## Cytotoxicity assays

The influence of the various formulations on the viability of AGS, Caco-2 and MDCK cells was evaluated by measuring the conversion of 3-(4,5-dimethylthiazol-2-yl)-2,5-diphenyltetrazolium bromide (MTT) to its insoluble formazan. Cells were seeded in 96-well microtiter plates ($10\times10^4$ cells/well) in 100 µL of complete medium. After 24 h, the medium was removed and replaced with 100 µL of the curcumin-loaded NCs diluted in minimal medium to final concentrations of 10, 25 and 50 µM curcumin. Free curcumin and unloaded NC and NE formulations were also tested in the same corresponding doses. After incubation for 4 h, the samples were removed and replaced with 100 µL MEM. We then added 25 µL MTT (5 mg/mL in PBS) and incubated the cells for another 4 h at 37 °C. The medium was removed, and 100 µL dimethyl sulfoxide (DMSO) was added to each well, followed by incubation for 30 min at 37 °C with orbital shaking in the dark. We then measured the absorbance at $\lambda = 490$ nm using a Safire A-5082 microplate reader. Cell viability was calculated as a percentage relative to the untreated control in MEM.

## Anti-adhesive effect against H. pylori

The quantitative anti-adhesion assay was performed by flow cytometry as previously described [26]. Briefly, H. pylori cells were grown for 48 h, collected from the agar plate, labeled with 1% (w/v) FITC in DMSO, washed, and incubated for 2 h at 37 °C in a blocking buffer (0.2% (w/v) BSA, 0.05% (v/v) Tween-20 in PBS pH 7.4) in the presence of formulations loaded with 10, 25 or 50 µM curcumin, and free curcumin as a control. After incubation, washing and re-suspension in antibiotic-free RPMI-1640 medium (containing 10% (v/v) fetal bovine serum and 1% (v/v) L-glutamine), H. pylori was incubated with AGS cells grown for 48 h in a six-well plate (cell density = $2\times10^5$ cell/well) for 1 h at 37 °C. Flow cytometry was carried out using a FACSCalibur device (Becton Dickinson, Heidelberg, Germany) at $\lambda_{ex}/\lambda_{em}$ = 485/538 nm to determine the number of cells with adherent, FITC-labeled bacteria, and the total fluorescence of each sample was expressed relative to the untreated control (maximum adherence). Free DexS40, DexS500, $CS_{HMC+30}$ and Lyz solutions were also tested for their anti-adhesive effects.

## Interaction between NCs and AGS monolayers

The ability of curcumin-loaded NCs to interact with AGS cell monolayers was tested by flow cytometry as described above for the quantitative curcumin uptake study. Briefly, AGS cells were grown for 48 h in a six-well plate (cell density = $2\times10^5$ cell/well) and then incubated for 1 h at 37 °C with curcumin-loaded NCs or free curcumin at a concentration of 25 µM diluted in complete medium. Unbound NCs were removed by washing with PBS. Cells were treated with trypsin, resuspended in RPMI-1640 medium and analyzed by flow cytometry to determine the percentage of fluorescent gated cells (FL1 green channel, $\lambda_{ex}$ = 488 and $\lambda_{em}$ = 510–545 nm). Curcumin uptake was calculated as the fold increase in green fluorescence relative to the untreated control.

## Confocal laser scanning microscopy

Interactions between H. pylori and gastric cells were investigated by confocal laser scanning microscopy (CLSM) using a Leica Microsystems (Wetzlar, Germany) TCS SP2 confocal system mounted on a Leica DM IRES inverted microscope. Cells and bacteria were treated as described above for the flow cytometry experiments. Briefly, FITC-labeled H. pylori were pre-treated with formulations containing 50 µM curcumin for 2 h, washed and incubated with cells for 1 h. The cells were fixed with 100 µL 4% (w/v) paraformaldehyde for 8 min. After three washes in PBS, the cells were permeabilized with 100 µL 0.1% (w/v) Triton-X100. Nuclei were stained using NucBlue Fixed Cell Staining Probes (Thermo Fisher Scientific, Waltham, MA, USA) by adding two drops per milliliter of medium. After 5 min, the samples were washed and stored in PBS for imaging.

Statistical analysis

The experimental results were reported as means ± standard deviations. Significant mean differences were determined by one-way analysis of variance (ANOVA) and independent T-sample tests using GraphPad Prism (GraphPad Software, San Diego, CA, USA).

## Results

Preparation and physicochemical characterization of nanocapsules

We prepared the oil core (NE-Lyz) by including Lyz in the aqueous phase (pH 4.5) during the spontaneous formation of an oil-in-water nanoemulsion. During the process of solvent displacement, the oil phase (containing lecithin, Mygliol, ethanol and acetone) was poured into the water phase, and the Lyz was adsorbed at the oil-in-water interface to produce the NE-Lyz homogeneous colloidal dispersion with a Z-average diameter of ~400 nm and a near-neutral ζ-potential (about +5.9 mV), as determined by DLS-NIBS and M3-PALS, respectively.

The NE-Lyz was then coated with two kinds of (negatively-charged) dextran sulfate (DexS40, Mw = 49 kDa, or DexS500, Mw = 632 kDa) by electrostatic interaction to form polymer-coated NCs. Rotavapor evaporation removed the organic solvents and part of the water. The variations in Z-average diameter and ζ-potential as a function of the DexS/Lyz charge ratio are shown in Figure 1.

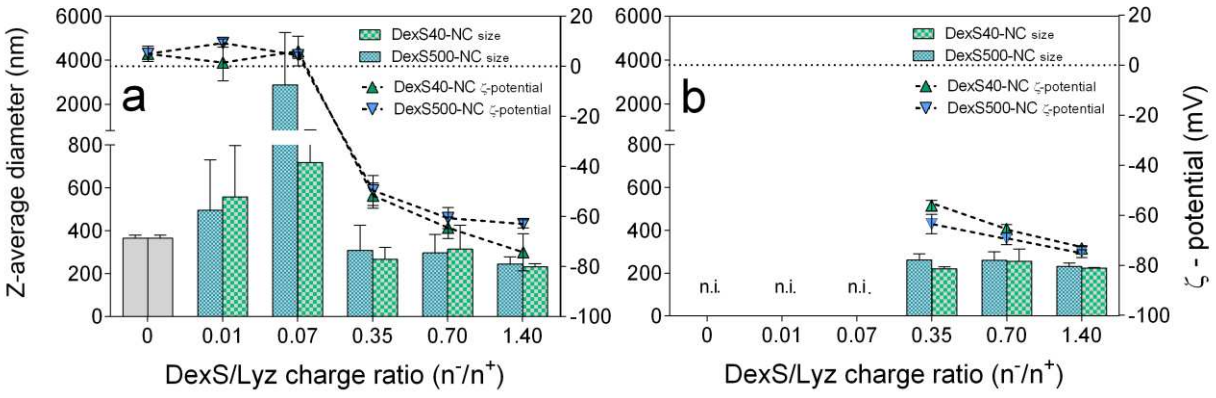


**Figure 1.** Variations in the Z-average diameter (bars) and ζ-potential (symbols) of NE-Lyz (0.75 mg/mL Lyz in the aqueous phase) coated with increasing concentrations of DexS40 or DexS500 (0.01, 0.1, 0.5, 1.0 and 2.0 mg/mL) expressed as the DexS/Lyz ($n^-/n^+$) charge ratio at pH 4.5 (a) before

and (b) after isolation by centrifugation (n.i. = not isolated). The Z-average diameter and ζ-potential were measured in MilliQ water and 1 mM KCl, respectively, at 25 °C (mean ± SD; n = 3).

At a DesS/Lyz $n^-/n^+$ charge ratio of 0.07, the polysaccharide-coated NCs had a Z-average diameter > 1000 nm for DexS500 and ~800 nm for DexS40. In both cases, the ζ-potential was the same as the uncoated NE-Lyz formulation. When the DesS/Lyz charge ratio was < 0.07, the amount of polysaccharide added was insufficient to change the ζ-potential of the NCs, suggesting incomplete coating of the NE-Lyz surface. For both forms of dextran sulfate, the ζ-potential became highly negative when the DesS/Lyz charge ratio was ≥ 0.35, but the Z-average diameter of the NCs was ~250 nm regardless of the type of polysaccharide. The ζ-potential profile was similar for both forms of the polysaccharide, although DexS40-NCs were slightly more negative when the DesS/Lyz charge ratio rose to 1.4. After centrifugation, only NCs with a DesS/Lyz charge ratio ≥ 0.35 could be isolated and the Z-average diameter and ζ-potential (Figure 1b) were similar to those before isolation (Figure 1a). NC prototypes with a DexS/Lyz charge ratio of 0.7 were selected for scaled-up production and curcumin loading. Pure NE was prepared using the same protocol, but Lyz was not included in the aqueous phase and the polysaccharide coating was omitted. A schematic representation of the process used to prepare the NE, DexS40-NC and DexS500-NC formulations is provided in Figure 2a. $CS_{HMC+30}$-NCs were prepared using the same protocol to determine the effect of a (positively-charged) chitosan coating on the biological properties of NCs. Uncoated NE-Lyz systems were not subsequently included in the experiments due to phase separation observed during short-term storage. The Z-average diameters of DexS40-NC, DexS500-NC and $CS_{HMC+30}$-NC formulations (loaded and unloaded) were significantly higher than NE, reflecting the presence of the polymeric shell. The positive ζ-potential of $CS_{HMC+30}$-NC confirmed the efficient adsorption of the cationic polysaccharide on the NE-Lyz surface. Table 1 summarizes the physical properties of the final selected prototype formulations (loaded with curcumin and unloaded controls). In keeping with the hypothesis that the polymers form a shell in the DexS40-NC and DexS500-NC formulations, TEM images revealed that the NCs are spherical particles with electron densities differing according to the type of formulation (Figure 2b). The NE formulation was easily distinguished by its naked electron-dense oil core, whereas the DexS-NCs featured a brighter surrounding layer. This layer was much wider and softer for the DexS500-NCs compared to the DexS40-NCs. Elemental analysis revealed the presence of sulfur solely in DexS40-NC and DexS500-NC formulations and not in the NE, as expected (Figure 2c).

**Table 1.** Physicochemical characterization of unloaded and curcumin-loaded NCs (DexS/Lyz $n^-/n^+$ charge ratio = 0.7). Values are means of three independent batches.

| Unloaded | | | | Curcumin-loaded | | | |
|---|---|---|---|---|---|---|---|
| Formulation | Size (d., nm) | PI[a] | ζ-potential (mV) | Formulation | Size (d., nm) | PI | ζ -potential (mV) |
| NE | 166 ± 18 | 0.113 | –59.4 ± 2.9 | cc-NE | 179 ± 24 | 0.125 | –55.7 ± 3 |
| NE-Lyz | 381 ± 11 | 0.097 | +5.9 ± 0.2 | cc-NE-Lyz | 353 ± 120 | 0.080 | –1.5 ± 6.7 |
| DexS40-NC | 198 ± 9 | 0.139 | –60.5 ± 6.5 | cc-DexS40-NC | 216 ± 11 | 0.096 | –53.5 ± 4.5 |
| DexS500-NC | 201 ± 10 | 0.112 | –55.7 ± 2.3 | cc-DexS500-NC | 220 ± 5 | 0.109 | –52.2 ± 5.7 |
| $CS_{HMC+30}$-NC | 187 ± 3 | 0.103 | +40.5 ± 2.9 | cc-$CS_{HMC+30}$-NC | 227 ± 25 | 0.141 | +23.8 ± 4.9 |

[a]PI = Polydispersity index

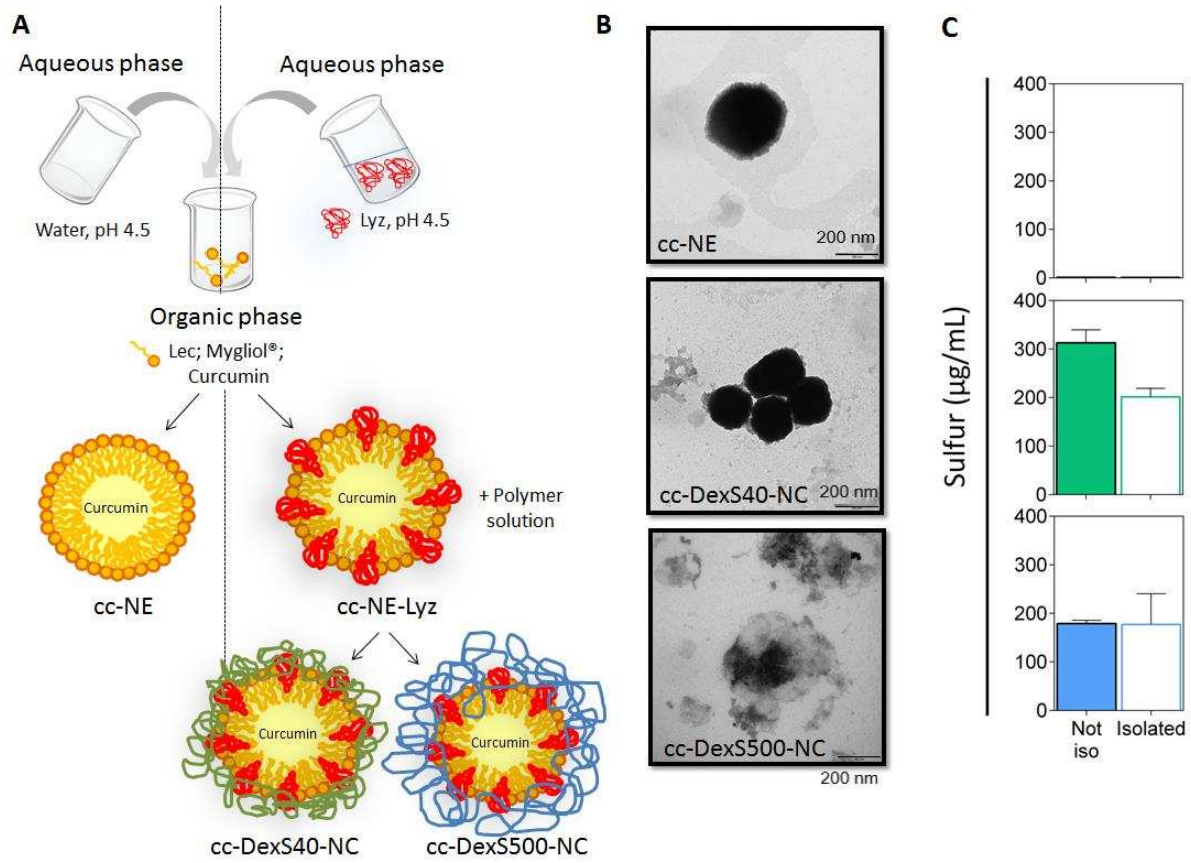


**Figure 2.** (a) Schematic representation of the NC preparation protocol. (b) Transmission electron micrographs of cc-NE, cc-DexS40-NC and cc-DexS500-NC formulations ($n^-/n^+$ charge ratio = 0.7) (magnification bar = 200 nm). (c) Elemental analysis to determine the sulfur content of the formulation before ("Not iso") and after isolation ("Isolated").

Stable curcumin-loaded NCs were successfully prepared, as evidenced by the visible homogeneous distribution of the deep-yellow color of curcumin in the colloidal dispersion. Although the inclusion of curcumin in the oil core caused a slight reduction in ζ-potential, in particular for the $CS_{HMC+30}$-NC formulation, in most cases there was no considerable variation in the Z-average diameter (Table 1). We also tested the activity of Lyz in the freshly-prepared NCs (both non-isolated and isolated), which revealed that Lyz retained its activity in all formulations, albeit to different degrees (Supporting Information, Fig. S1). In contrast to our expectations, the inclusion of Lyz in the $CS_{HMC+30}$-NC formulation did not trigger the autodigestion of the chitosan shell, despite the well-known ability of Lyz to hydrolyze chitosan with a high degree of acetylation [27].

Electrokinetic properties as a function of pH

The physicochemical characteristics of the NCs were studied in more detail by investigating their surface electrical properties as a function of the coating. Figure 3a shows the ζ-potential of NCs at different pH values, consistent with the functional group exposed on the surface. The simple cc-NE formulation showed a neutral point at pH ~3.0 in keeping with the exposure of phosphatidylcholine phosphate groups, representing the major component of lecithin Epikuron 145v ($pK_a$ ~3 and ~4), at the emulsion interface. Below pH 3.0, when the phosphate groups of cc-NE are mostly protonated, the net positive charge of the choline residue dominates, conferring an overall positive ζ-potential. For the cc-DexS-NC formulations, the sulfate groups ($pK_a$ ~1.5–2) contribute most of the negative charge, and the ζ-potential of cc-DexS40-NC thus remains strongly negative even at pH ~1.2, whereas cc-DexS500-NC approaches a near-neutral ζ-potential at pH < 2.0. For the cc-$CS_{HMC+30}$-NC formulation, the amino groups contribute to a positive charge under acidic pH conditions, and the ζ-potential thus goes from positive to negative as the pH declines, passing through an isoelectric point at pH ~8.0. The Z-average diameter of all the NC formulations increased when the pH was equivalent to the isoelectric point, consistent with the charge compensation phenomenon (star symbols in Figure 3b).

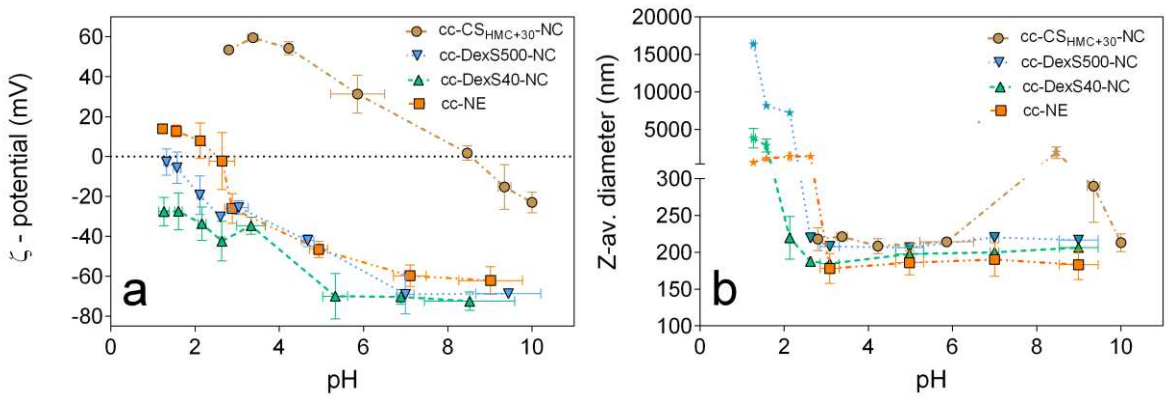


**Figure 3.** Variation of (a) the ζ-potential and (b) the Z-average diameter as a function of pH for the different NCs and NE. Stars indicate Z-average diameters that do not meet the instrument's size determination quality criteria (mean ± SD; n = 3).

Efficiency of curcumin encapsulation

Centrifugation of the curcumin-loaded formulations yielded three phases: a creamy top layer containing the NCs, a subnatant comprising excess dissolved components, and a pellet comprising

excess DexS/Lyz complexes. Curcumin was unevenly distributed among the three phases, as shown in Table 2.

**Table 2.** Distribution of curcumin as a measure of association efficiency (%) in the three phases of each formulation after isolation.

| Formulation | Isolated NCs (%) | Subnatant (%) | Pellet (%) | Overall encapsulated concentration (μM) |
|---|---|---|---|---|
| cc-NE | 69.3 ± 1.9 | 26.0 ± 1.4 | 4.7 ± 1.0 | 125 ± 2 |
| cc-DexS40-NC | 72.4 ± 5.6 | 13.8 ± 4.5 | 13.7 ± 3.3 | 146 ± 8 |
| cc-DexS500-NC | 68.4 ± 3.7 | 16.7 ± 3.7 | 14.9 ± 2.5 | 141 ± 6 |
| cc-$CS_{HMC+30}$-NC | 73.3 ± 2.7 | 21.3 ± 0.4 | 5.4 ± 3.1 | 133 ± 1 |

Before isolation, excess DexS/Lyz complexes are homogeneously dispersed together with the NCs in a colloid and contribute to a narrow Gaussian distribution of particle sizes as shown by the low polydispersity index (PI) of < 0.1 (Table 1). These complexes sequester curcumin, and therefore reduce the quantity of curcumin found in the subnatant by ~50% when the cc-DexS-NC formulations are compared to cc-NE and cc-$CS_{HMC+30}$-NC. However, they do not interfere with the loading capacity of the isolated NCs, which sequester ~70% of the curcumin in all formulations. Given that curcumin is only sparingly soluble in water (0.5 μM), the large amount of free curcumin found in the subnatant of the NE and cc-$CS_{HMC+30}$-NC formulations suggests that free lecithin may influence the curcumin partition coefficient during centrifugation.

Stability in physiologically-relevant media

The stability of the formulations under conditions that simulate the gastrointestinal tract ($SGF_{sp}$, mucin, and PBS pH 6.8) and in cellular medium (supplemented RPMI-1640) is summarized in Figure 4 as a function of the particle Z-average diameter (bars) and the derived count rate (DCR, symbols) at time points 0, 4 and 24 h. The Z-average diameter of cc-DexS500-NC (Figure 4a) and cc-DexS40-NC (Figure 4b) in $SGF_{sp}$ increased during the first 4 h, concomitant with the dramatic reduction in

the DCR. In contrast, the cc-NE formulation remained stable in all media (Figure 4c) whereas the cc-$CS_{HMC+30}$-NC formulation was much less stable in PBS pH 6.8 than in water, as shown by the lower DCR at time point 0 (Figure 4d). In supplemented RPMI-1640 medium, all formulations became progressively smaller during incubation, accompanied by an increase in the DCR. In the presence of mucin (1 mg/mL), the Z-average diameter and DCR of all four formulations remained essentially constant for 4 h.

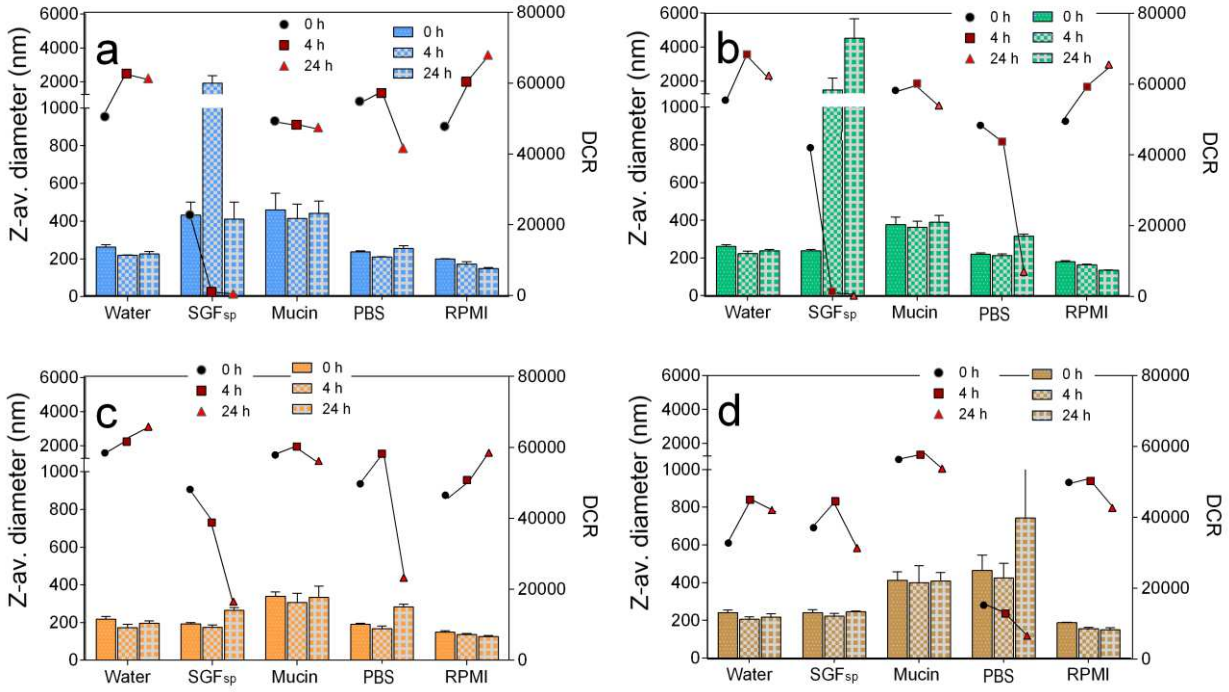


**Figure 4.** Variation in the Z-average diameter (bars) and derived count rate (symbols) during incubation in water and various physiologically-relevant media at time 0, 4 and 24 h at 37 °C: (a) cc-DexS500-NC; (b) cc-DexS40-NC; (c) cc-NE; (d) cc-$CS_{HMC+30}$-NC (mean ± SD; n = 3).

## Interaction with $PLA_2$

To gain insight into the NC degradation mechanisms in the gastrointestinal tract and the potential for NCs to interact with H. pylori adhesins, we incubated the formulations with $PLA_2$ (Figure 5a). When treated with the same amount of $PLA_2$, the relative absorbance of cc-NE, cc-DexS500-NC and cc-DexS40-NC declined at different rates with respect to the controls, and reached a minimum value after 900 s in the order cc-DexS40-NC > cc-NE > cc-DexS500-NC. For cc-DexS500 and cc-DexS40, the reduction in relative absorbance was consistent with the declining particle size, whereas there was no difference in size between cc-NE and the control (Figure 5b). Interestingly, the major difference between formulations was the rate at which absorbance decreased during the early stages of the

reaction (< 200 s), with the steepness of the slopes ranked as follows: cc-NE > cc-DexS500-NC > cc-DexS40-NC. During the later stages (> 200 s), the relative absorbance remained constant for cc-NE, but declined steadily for cc-DexS40-NC and cc-DexS500-NC. Conversely, the cc-$CS_{HMC+30}$-NC system exhibited a monotonic and essentially linear increase in relative absorbance.

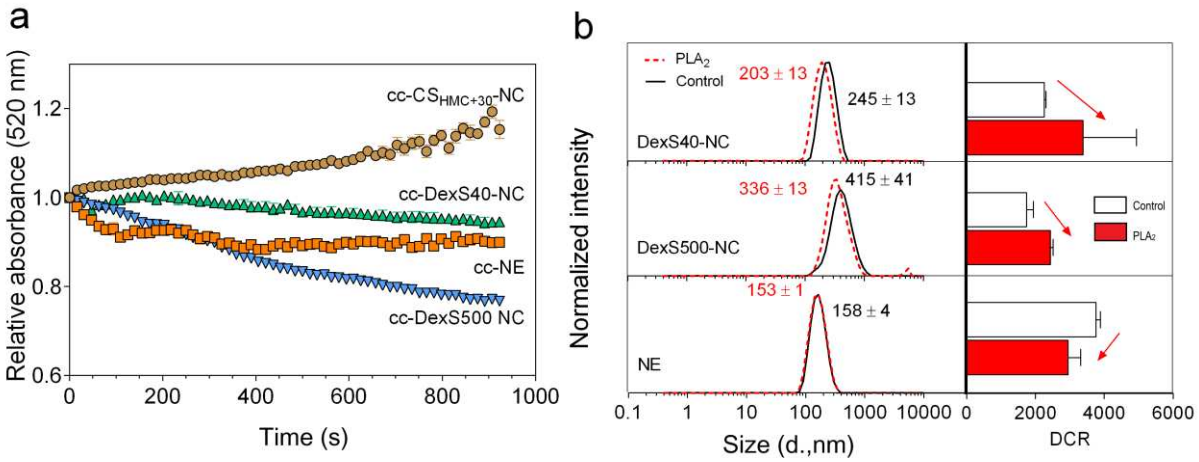


**Figure 5.** (a) Relative absorbance (λ=520 nm) during the incubation of the formulations with $PLA_2$ (values normalized to time point 0). (b) Z-average diameter and derived count rate endpoint values following the incubation of cc-DexS40-NC, cc-DexS500-NC and cc-NE with $PLA_2$ (initial, control and endpoint $PLA_2$, as shown in the labels). Conditions for the enzymatic reaction: 5 mM $CaCl_2$ and 1 mM EDTA (pH 8) for ~15 min at 37 °C (mean ± SD; n = 4).

Figure 5b also shows a decline in the relative absorbance and DCR of the sample collected after the kinetic measurements. In the control treatments, the Z-average diameters of the cc-NE and cc-DexS40-NC formulations remained similar to the original values for these formulations, whereas there was a slight increase for cc-DexS500-NC (Table 1). However, the Z-average diameters of both cc-DexS40-NC and cc-DexS500-NC declined significantly in the presence of $PLA_2$, accompanied by an increase in the DCR, in keeping with the progressive reduction in turbidity, suggesting that the major contribution to the scattered light was the particle size. In the case of cc-$CS_{HMC+30}$-NC, intensity and DCR values could not be recorded due to the high polydispersity of the sample (PI ~1) and the poor quality of the measurements, indicating that these NCs are unstable in the reaction buffer both in the presence and absence of $PLA_2$.

Effect of NCs on the viability of eukaryotic cells

The influence of curcumin-loaded NCs on the viability of MDCK-C7, Caco-2 and AGS cell lines was tested by culturing the cells in MEM and then exposing them to the NCs for 4 h at 37 °C, followed by an MTT assay. Figure 6 shows the dose-dependent effect of free curcumin and curcumin-loaded NCs at identical curcumin doses. Notably, free curcumin solution induced cytotoxic effects in all three cell lines, albeit only at 50 µM in MDCK-C7 cells (Figure 6a) but with a clear dose-dependent effect in Caco-2 and AGS cells (Figures 6b and 6c). However, the inclusion of curcumin in the NCs abrogated these effects in all three cell lines, even at the highest concentration (50 µM), and in some cases even promoted a slight increase in cell viability. MDCK cells responded similarly to all NCs except cc-NE, which showed increased cell viability, regardless of curcumin dose (Figure 6a). Similar behavior was observed for the control NE formulation lacking curcumin (lower panel, Figure 6a). In Caco-2 cells, cc-NE and cc-$CS_{HMC+30}$-NC enhanced cell viability whereas cc-DexS400-NC and cc-DexS500-NC reduced viability by 80% and 50%, respectively, also regardless of the curcumin dose. Moreover, DexS500-NC was cytotoxic even in the absence of curcumin (lower panel, Figure 6b). Note that, in AGS cells, as the curcumin dose increased in the different formulations from 10 to 50 µM, the cell viability increased from ~70% to ~120–130% for cc-$CS_{HMC+30}$-NC and cc-DexS40-NC, from ~50% to ~70% for cc-DexS500-N, and remained unchanged for the cc-NE formulations. Interestingly, the AGS cell line was more sensitive to the unloaded formulations, given that all such treatments reduced cell viability by up to 50% regardless of the dose.

Interaction between NCs and AGS cells

Based on the principle of interaction with immobilized mucin, the green fluorescence of curcumin was used to quantify the interaction between NCs and monolayers of AGS cells by flow cytometry (Figure 7). Interestingly, the cells treated with the formulations carrying a negative net charge (cc-NE, cc-DexS4-NC and cc-DexS500-NC) showed significantly higher fluorescence values than those treated with the positively-charged formulation (cc-$CS_{HMC+30}$). However, the uptake of curcumin by the cells was much higher when they were presented with the free compound rather than the NC formulations.

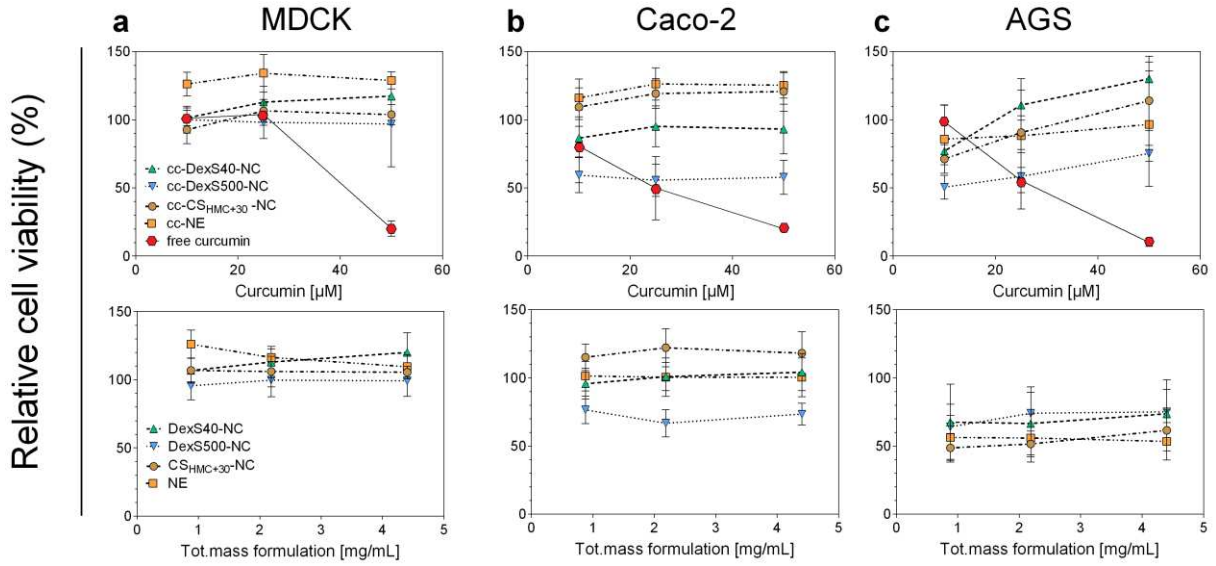


**Figure 6.** Effect of the NC formulations and free curcumin on relative cell viability, determined by MTT assay in (**a**) MDCK-C7, (**b**) Caco-2 and (**c**) AGS cells after 4 h incubation in MEM. Upper panel: treatment of the cells with NCs with increasing concentrations of curcumin. Lower panel: the corresponding results for the effects of unloaded formulations at equivalent doses as the curcumin-loaded NCs. Values are means ± SD (n = 3 independent experiments, 8 replicates each) relative to untreated cells.

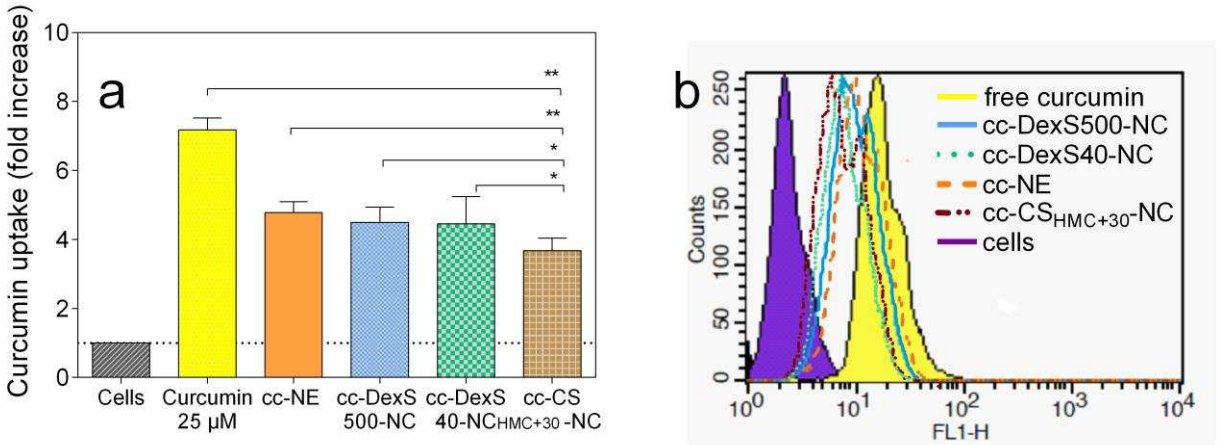


**Figure 7. (a**) Interaction of AGS cells after 1 h of incubation with free curcumin (25 μM) and with curcumin-loaded NCs (25 μM curcumin) measured by flow cytometry, showing the increasing percentage of gated green fluorescent cells relative to untreated control (autofluorescence). (**b**) Histogram of AGS cells treated with the different formulations (mean ± SD; n = 3 independent experiments with 2 replicates each; $^{*}p < 0.05$; $^{**}p < 0.01$).

Interference of NCs with the adhesion of H. pylori to AGS cells

The ability of FITC-labeled H. pylori to adhere to an 80% confluent monolayer of AGS cells was quantified by flow cytometry following the pretreatment of the bacteria with curcumin-loaded NCs. The results were expressed as percentage adhesion relative to the untreated control (set to 100%). Figure 8 shows the dose-dependent reduction in the adhesion of H. pylori following pretreatment with the formulations (Figure 8a) or their free components (Figure 8b), together with the flow cytometry histograms (Figure 8c). The anti-adhesive properties of the NCs were ranked as follows: cc-DexS40-NC >> cc-DexS500-NC > cc-NE. In contrast, the positively-charged cc-$CS_{HMC+30}$-NC formulation promoted the attachment of bacteria to the AGS cells, as did the free chitosan solution at an equivalent concentration to that found in the NCs. Free curcumin significantly inhibited adhesion only at the highest equivalent dose (50 µM).

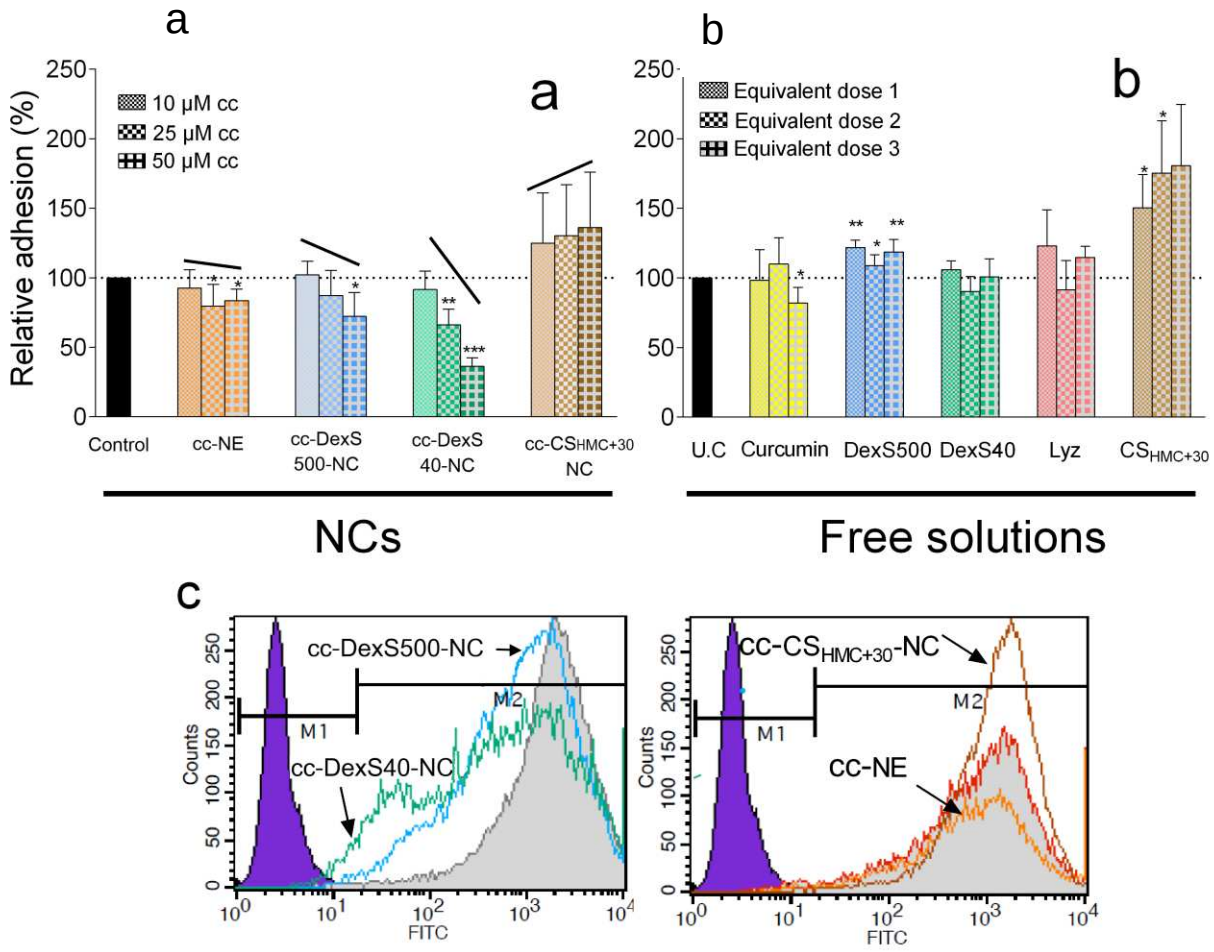


**Figure 8.** Relative adhesion of FITC-labelled H. pylori to AGS cells as determined by flow cytometry after pre-incubation of the bacteria (in 0.2% (w/v) BSA, 0.05% (v/v) Tween-20 in PBS pH 7.4, 2 h, 37 °C) with varying concentrations of: (a) curcumin-loaded NCs and (b) free solutions of the components at the same doses (equivalent dose 1 = 0.04 mg/mL DexS40 or DexS500 or $CS_{HMC+30}$, 0.1 mg/mL Lyz or 10 µM curcumin; equivalent dose 2 = 0.1 mg/mL DexS 40 or DexS500 or $CS_{HMC+30}$, 0.25 mg/mL Lyz or 25 µM curcumin; equivalent dose 3 = 0.2 mg/mL DexS 40 or DexS500 or $CS_{HMC+30}$, 0.5 mg/mL Lyz or 50 µM curcumin). (c) Representative flow cytometry histograms of AGS cells (violet shaded area) AGS + H. pylori (gray shaded area) and AGS + H. pylori treated with curcumin-loaded NCs (50 µM curcumin). Data in (a) and (b) are relative to untreated control (mean ± SD; n = 3 independent experiments with 2 replicates each; $^{*}p < 0.05$; $^{**}p < 0.01$).

H.pylori-cell interaction by confocal laser scanning microscopy (CLSM)

CLSM images recorded upon incubation of bacteria and the different formulations revealed that untreated FITC-labeled H. pylori efficiently binds to the membrane of AGS cells as can see by the green fluorescence occurring all around the shape of the cells (Supporting Information Figure S5). Treatment with the different nanoformulations revealed that the bacterial adhesion was affected, however, a quantitative assessment was not possible and the fluorescence of the NC formulations

themselves can interfere with the assay. In the case of $CS_{HMC+30}$ NC, large aggregates were visible in the proximity of the AGS cells, suggesting a bacterial clustering effect.

## Discussion

Antibiotic-free options for the treatment of H. pylori infections are needed urgently to prevent the further spread of drug-resistant strains, and nanomaterials that persist or diffuse within the mucus layer of the stomach are ideal for this purpose. Efficacious formulations should meet at least the following three criteria: (a) they should increase the residence time in the stomach by interacting with mucins; (b) they should inhibit bacterial adhesion and/or communication thus exploiting a local mode of action; and (c) they should release small molecules such as curcumin that help to prevent gastric ulcers and inflammation. Our previous studies have shown that both anionic polysaccharides such as dextran sulfate and cationic ones such as chitosan can interact with mucin [11], and some of these can also modulate adhesive interactions with H. pylori. We therefore prepared NC formulations based on NE-Lyz (with or without curcumin) coated with different forms of dextran sulfate or chitosan, and tested their ability to disrupt the adhesion between H. pylori and gastric epithelial cells.

NC formulations can be prepared using a spontaneous emulsification solvent displacement method [24, 28] in which a negatively-charged oily core stabilized by the anionic surfactant lecithin is coated with cationic polymers such as chitosan [24] or poly-L-asparagine [29]. The use of synthetic cationic surfactants instead provides the means to coat NCs with anionic polymers such as kappa-carrageenan [30] or hyaluronan [31], but this approach is restricted by the limited availability of pharmaceutical-grade cationic surfactants [32]. Strategies to overcome this limitation include the use of non-ionic surfactants with coacervated ions [33] and the layer-by-layer technique involving sequential coating with positively and negatively charged polyelectrolytes [34-39]. We addressed the challenge by including Lyz as a non-toxic, amphiphilic protein that acts as a co-surfactant together with lecithin during the formation of a primary emulsion (NE-Lyz). This allowed the preparation of NC formulations coated with anionic dextran sulfate. Lyz is a small protein (14 kDa, dimensions 4.5×3×3 nm) with a high isoelectric point of 11.16, thus conferring a net positive charge across a broad pH range [40,41] and facilitating its absorption at the oil-in-water interface [42]. Based on the effect of Lyz and other proteins on NC properties in earlier studies [43-45], we selected a concentration of 0.75 mg/mL to ensure that the negatively charged lecithin core of our NCs was covered but not overwhelmed, in agreement with the behavior of chitosan when added at varying concentrations to the primary NE-Lyz emulsion (Supporting Information Figure S2), as also described for SDS-stabilized chitosan-NCs [31].

The composition of the DexS500-NC (but not DexS40-NC) formulations was optimized based on the change in ζ-potential of NE-Lyz when adding varying amounts of dextran sulfate, expressed as the DexS/Lyz $n^-/n^+$ charge ratio (Figure 1). At low charge ratios ($n^-/n^+ < 0.07$) the ζ-potential was near neutral, suggesting that Lyz is not homogeneously distributed on the surface of the emulsion but may be intercalated in the phospholipid monolayer, exposing its positively charged groups. This indicates that the absorption of the polysaccharide to the particle surface does not depend on the polymer chain length when coverage is sparse [46]. In contrast, when dextran sulfate was added at high charge ratios ($n^-/n^+ > 0.07$), the coverage was sufficient for both forms of the polysaccharide to induce a high negative ζ-potential (approximately –55 to –60 mV; Z-average diameter ~200 nm, low polydispersity). No major size differences were observed by TEM, but there were significant differences in morphology, including a marked contrast between the electron-dense oily core and the surrounding shell structure for DexS500-NC but not DexS40-NC, which may reflect differences in the packing of the long and short polymer chains [47, 48]. These differences did not influence the capacity to load curcumin in the oily core (Table 2) although there was evidence for greater affinity between curcumin and the DexS40-NC/DexS500-NC colloidal suspensions.

The pH-dependent ζ-potential profile revealed that DexS40-NC and DexS500-NC have a negative ζ-potential at pH < 3.0, confirming the presence of sulfate groups on the surface (Figure 3). However, DexS500-NC was more effectively neutralized at low pH (~1.5) than DexS40-NC, which may reflect the lower flexibility of the smaller polymer chains restricting the accessibility of the positively charged functional groups by making the coating more compact [11], consistent with the TEM data (Figure 2b). The expanded coating of the DexS500-NC formulation may allow more access for protonation to facilitate the neutralization of the NC surface. The pH titration profiles could also explain why neither DexS40-NC nor DexS500-NC were stable in $SGF_{sp}$ resulting in them gaining size and experiencing a reduction in the DCR during the first 4 h of incubation, whereas $CS_{HMC+30}$-NC and NE maintained a fairly constant profile. This may indicate that the presence of NaCl (equivalent to 34 mM) in the $SGF_{sp}$ stabilizes the system, as previously observed in oil-core colloidal nanocapsules at < 50 mM NaCl [48]. Although the in vitro stability studies may predict that neither DexS40-NC nor DexS500-NC would be suitable for direct in vivo administration to the stomach, different dosage forms could be developed (such as freeze/spray-dried powders or gel capsules) to protect the formulations from contact with gastric juice before they reach the gastric mucus layer. All formulations were stable in complete RPMI-1640 medium at pH 7.4 and also in PBS at pH 6.8 in the presence of mucin, where the ζ-potential was either highly negative or moderately positive, enhancing electrostatic colloidal stabilization.

To gain insight into biological behavior of the NCs, we investigated their degradation by $PLA_2$, which hydrolyzes the sn-2 ester bond of phospholipids according to their structure and organization, favoring negatively charged lipids [49], monolayers [50] and liopolymers such as polyethylene glycol [51,52]. We found that $PLA_2$ interacted more readily with the smaller, negatively charged NE, which has a large surface area. There was little activity against DexS40-NC, probably reflecting the compact structure of its coating, but a more consistent effect against the more expansive DexS500-NC coating, resulting in a monotonic decline in turbidity, as observed for a lipid-nanoemulsion digested with $PLA_2$ in simulated intestinal fluid containing 5 mM $Ca^{2+}$ [53]. Moreover, the release of hydrolysis products from structured phospholipid assemblies may promote structural rearrangement [50]. This may explain why NE maintained a constant size in the presence of $PLA_2$ whereas DexS40-NC and DexS500-NC became smaller, as a portion of the DexS/Lyz complex on the surface was stripped away. The $CS_{HMC+30}$-NCs behaved in a distinct manner despite their general poor stability, probably because interaction with the enzyme promoted aggregation due to bridging phenomena.

We also tested the effect of curcumin-loaded NC and NE formulations on the viability of AGS, Caco-2 and MDCK-C7 cells. AGS and Caco-2 are carcinoma lines from the human gastrointestinal tract, and we observed the dose-dependent cytotoxic effect of free and encapsulated curcumin after 4 h exposure. The dose-dependent inhibition of carcinoma cell proliferation by curcumin is associated with the induction of apoptosis, with $IC_{50}$ values of ~22 and ~10 µM against AGS and Caco-2 cells, respectively [54,55]. Even in absence of curcumin, DexS500-NC was more cytotoxic than DexS40-NC towards Caco-2 cells due to their higher sensitivity towards the higher-molecular-weight dextran sulfate [56]. In contrast, cytotoxicity against the canine kidney cell line MDCK-C7 was observed solely at the highest curcumin concentration of 50 µM, reflecting the general resistance of kidney cells to curcumin [57]. We found that the cytotoxicity of free curcumin was attenuated by encapsulation in the NCs, which contrasts with previous studies using nanoparticles, nanocapsules and micelles, possibly because these studies involved different formulations, cell lines and incubation times [55,58,59]. Curcumin has a cytoprotective effect due to its antioxidant activity [60] but can also induce mitochondrial dysfunction in AGS cells and the intestinal epithelial cell line HT-29 [54] by opening the mitochondrial permeability transition pore (PTP), although the latter activity is inhibited by hydrophobic substrates [60]. We found that the dose-dependent cytotoxicity of free curcumin in AGS cells was ameliorated in the NC formulation by an increase in metabolic activity, perhaps because the PTP activity is blocked in this context.

Regarding the safety of dextran sulfate, the repeated administration of high concentrations (2–10% w/v) of the polysaccharide (Mw 5000–54,000) in drinking water induces colitis in mice and rats [61].

In contrast, the concentration of dextran sulfate in the antiadhesive NC formulations was at least two orders of magnitude lower (0.02% w/v) than that known to induce gastrointestinal side effects in animals. Indeed, dextran sulfate is increasingly considered as an excipient for food and pharmaceutical formulations [62,63]. In addition, the developed NC formulation can be seen as versatile platform opening the possibility of including other negatively-charged polyanions with potential antiadhesive activity (e.g. fucoidan, okra pectins, etc.). What is more, besides curcumin, other lipophilic active pharmaceutical and natural ingredients could also be co-loaded at the oily core of other new formulations able to aid in H. pylori eradication.

The interaction between H. pylori and gastric carcinoma cell line MKN45 can be blocked and reversed by exposure to chitosan microspheres, with preferential inhibition at pH 6 regardless of the bacterial strain/adhesin profile [64]. However, the properties of nanomaterials and microparticles often differ. Accordingly, we found that the small negative charge of H. pylori at pH 7.4 (ζ-potential of approximately –7 mV) [65] attracted the $CS_{HMC+30}$-NC formulation (ζ-potential of approximately +20 mV at pH 7.4), reflecting the formation of electrostatic interactions between NCs and bacteria, in line with our own studies [66] and those of others [67]. The mixture of H. pylori and $CS_{HMC+30}$-NC was difficult to resuspend after incubation for 2 h, probably reflecting the formation of aggregates, which may have generated false positive fluorescent signals in the adhesion assay with AGS cells [68]. This may explain why the CLSM images in the case of H. pylori treated with $CS_{HMC+30}$-NC did show fluorescence and a large cluster around a single cell (Supporting Information Fig. S5). Chitosan-coated NCs may, therefore, influence the viability and morphological adaptation of the bacteria [69], making them unsuitable for adhesion assays, although we observed no such toxicity in disc diffusion assays (Supporting Information, Fig. S3).

In contrast to chitosan systems, negatively charged NCs are not thought to promote bacterial clustering [66,67] but they can interact with H. pylori and prevent its adhesion in situ [70]. Negatively charged polysaccharides inhibit the adhesion of H. pylori to gastric adenocarcinoma cells and human tissue sections due to the high content of uronic acid residues [13, 16], low degree of chain branching [13], high molecular weight and presence of sulfated groups [18]. Dextran sulfate can trigger the dissociation of H. pylori-mucin complexes and inhibit adhesion to gastric adenocarcinoma cells in a urease-dependent manner at low pH [22], inhibit the binding of heparan sulfate to its receptor on the H. pylori surface at pH 4.5 [71], and inhibit H. pylori binding to gastric mucin at pH < 4.0 [18]. We found that free DexS40 and DexS500 did not inhibit H. pylori adhesion to AGS cells but cc-DexS40-NC and cc-DexS500-NC inhibited bacterial adhesion by up to ~60% even at pH 7.4. Unloaded DexS40-NC and DexS500-NC also inhibited adhesion but significantly less than the curcumin-loaded

formulations, suggesting curcumin may contribute to the observed anti-adhesive properties (Supporting information, Figure S4).

## Conclusion

We developed a novel Lyz/lecithin-stabilized NE that can be coated with anionic polysaccharides, avoiding the use of cationic surfactants. The presence of the different polymeric coats was confirmed by electrokinetic analysis, morphological visualization, elemental analysis, and stability testing, and biological activity was also verified. We found that NCs coated with low-molecular-weight dextran sulfate (DexS40-NC) were less cytotoxic towards human gastric carcinoma cells than counterparts coated with high-molecular-weight dextran sulfate (DexS500-NC). The DexS40-NC and DexS500-NC formulations significantly inhibited the adhesion of H. pylori to gastric cells, but a bulk solution of dextran sulfate did not achieve this anti-adhesive effect. To the best of our knowledge, this is the first in vitro proof of concept that dextran sulfate-coated NCs can inhibit the adhesion of H. pylori to stomach cells, at least in the context of in vitro cell monolayers. Studies in vivo using infected mice are required to gain mechanistic insights and establish the efficacy of anti-adhesive formulations, as well as to demonstrate tolerability and safety. Given that the formulations described herein can be adapted to contain only food-grade ingredients, we anticipate a feasible roadmap to aproval as a food supplement in the future. The antiadhesive formulations could also be used to facilitate erradication quadruple therapy, by making it more difficult for the bacteria (in the presence of antibiotics) to hide underneath the mucus layer where antibiotics do not penetrate effectively, thus making them more sensitive to current therapeutic doses. One shortcoming of the H. pylori-AGS stomach cells model is that it does not account for the presence of mucin in vivo. However, we propose that the presence of dextran sulfate on the surface of the NCs may help to modulate the binding of H. pylori mediated by the intertaction between bacterial adhesin BabA and mucin MUC5A [72]. Future studies should address the mucoadshesive or mucodiffusive behavior of the NC formulations. We conclude that curcumin-loaded oil-core NCs coated in dextran sulfate have the size, composition and surface characteristics necessary to develop novel antibiotic-free strategies to prevent and treat H. pylori infections, particularly in settings affected by the increasing prevalence of antibiotic resistance.

## Supporting Information

The Supporting Information is available free of charge on the ACS Publication website at DOI:

- Lysozyme activity, ζ-potential titration of nanoemulsions, agar diffusion inhibition toxicity assays in H. pylori, relative adhesion of FITC-labeled H. pylori on AGS cells, and CLSM images

**Acknowledgements**

We acknowledge financial support from the German Research Foundation DFG (Project GRK 1549 International Research Training Group 'Molecular and Cellular GlycoSciences'). We are indebted to Susana M. Pereira and Pavani Ayinampudi for their valuable technical assistance. We also thank Dr. Richard M. Twyman for editing the manuscript.

**References**

(1) Hooi, J. K. Y.; Lai, W. Y.; Ng, W. K.; Suen, M. M. Y.; Underwood, F. E.; Tanyingoh, D.; Malfertheiner, P.; Graham, D. Y.; Wong, V. W. S.; Wu, J. C. Y.; Chan, Francis K.L.; Sung, Joseph J.Y.; Kaplan, Gilaad G.; Ng, Siew C. Global Prevalence of Helicobacter pylori Infection: Systematic Review and Meta-Analysis. Gastroenterology **2017**, 153 (2), 420–429. https://doi.org/10.1053/j.gastro.2017.04.022.

(2) Kim, S. S.; Ruiz, V. E.; Carroll, J. D.; Moss, S. F. Helicobacter pylori in the Pathogenesis of Gastric Cancer and Gastric Lymphoma. Cancer Lett. **2011**, 305 (2), 228–238. https://doi.org/10.1016/j.canlet.2010.07.014.

(3) Odenbreit, S., Adherence properties of Helicobacter pylori: Impact on pathogenesis and adaptation to the host. Int. J. Med. Microbiol. **2005**, 295(5), 317-324.

(4) Montecucco, C.; Rappuoli R. Living Dangerously: How Helicobacter pylori Survives in the Human Stomach. Nat. Rev. Mol. Cell Bio. **2001**, 2(6), 457-466.

(5) Malfertheiner, P., Megraud, F., O'Morain, C., Gisbert, J. P., Kuipers, E. J., Axon, A., Bazzoli, F., Gasbarrini, A.; Atherton, J.; Graham, D. Y.; Hunt, R.; Moayyedi, P.; Rokkas, T.; Rugge, M.; Selgrad, M.; Suerbaum, S.; Sugano, K.; El-Omar, E.; Agreus, L.; Andersen, L. P.; Coelho, L.; Delchier, J. C.; Di Mario, F.; Dinis-Ribeiro, M.; Fischbach, W.; Flahou, B.; Fock, K. M.; Gasbarrini, G.; Gensini, G.; Goh, K. L.; Herrero, R.; Kupcinskas, L.; Lanas, A.; Leja, M.; Machado, J. C.; Mahachai, V.; Milosavljevic, T.; Niv, Y.; Ristimaki, A.; Tepes, B.; Vaira, D.; Vieth, M.; You, W. You, W. Management of Helicobacter pylori Infection-the Maastricht V/Florence Consensus Report. Gut **2017,** 66(1), 6–30. https://doi.org/10.1136/gutjnl-2016-312288.

(6) Shah, S.; Qaqish, R.; Patel, V.; Amiji, M., Evaluation of the Factors Influencing Stomach-Specific Delivery of Antibacterial Agents for Helicobacter pylori Infection. J. Pharm. Pharmacol. **1999,** 51(6), 667-72.

(7) Santos, R. S.; Dakwar, G. R.; Zagato, E.; Brans, T.; Figueiredo, C.; Raemdonck, K.; Azevedo, N. F.; De Smedt, S. C.; Braeckmans, K. Intracellular Delivery of Oligonucleotides in Helicobacter pylori by Fusogenic Liposomes in the Presence of Gastric Mucus. Biomaterials **2017,** 138, 1-12. https://doi.org/10.1016/j.biomaterials.2017.05.029.

(8) Lopes, D.; Nunes, C.; Martins, M. C. L.; Sarmento, B.; Reis, S. Eradication of Helicobacter pylori: Past, Present and Future. J. Control. Release **2014**, 189, 169–186. https://doi.org/10.1016/j.jconrel.2014.06.020.

(9) Ensign, L.M.; Cone R.;, Hanes J. Oral Drug Delivery with Polymeric Nanoparticles: The Gastrointestinal Mucus Barriers. Adv. Drug Deliver. Rev. **2012**, 64(6), 557-570.

(10) Mackie, A. R.; Goycoolea, F. M.; Menchicchi, B.; Caramella, C. M.; Saporito, F.; Lee, S.; Stephansen, K.; Chronakis, I. S.; Hiorth, M.; Adamczak, M.; Waldner, M.; Nielsen, H.M.; Marcelloni, L. Innovative Methods and Applications in Mucoadhesion Research. Macromol. Biosci. **2017**, 17 (8), 1–32. https://doi.org/10.1002/mabi.201600534.

(11) Menchicchi, B.; Fuenzalida, J. P.; Hensel, A.; Swamy, M. J.; David, L.; Rochas, C.; Goycoolea, F. M. Biophysical Analysis of the Molecular Interactions between Polysaccharides and Mucin. Biomacromolecules **2015**, 16 (3), 924–935. https://doi.org/10.1021/bm501832y.

(12) Menchicchi, B.; Hensel, A.; Goycoolea, F. M. Polysaccharides as Bacterial Antiadhesive Agents and "Smart" Constituents for Improved Drug Delivery Systems Against Helicobacter pylori Infection. Curr. Pharm. Des. **2015**, 21, 4888–4906. . https://doi.org/10.2174/1381612821666150820104028.

(13) Lengsfeld, C.; Titgemeyer, F.; Faller, G.; Hensel, A. Glycosylated Compounds from Okra Inhibit Adhesion of Helicobacter pylori to Human Gastric Mucosa. J. Agric. Food Chem. **2004**, 52 (6), 1495–1503. https://doi.org/10.1021/jf030666n.

(14) Messing, J.; Thöle, C.; Niehues, M.; Shevtsova, A.; Glocker, E.; Borén, T.; Hensel, A. Antiadhesive Properties of Abelmoschus esculentus (Okra) Immature Fruit Extract against Helicobacter pylori Adhesion. PLoS One **2014**, 9 (1) e84836. https://doi.org/10.1371/journal.pone.0084836.

(15) Belogortseva, N.I.; Yoon J.Y.; Kim K.H. Inhibition of Helicobacter pylori hemagglutination by polysaccharide fractions from roots of Panax ginseng. Planta Med, **2000.** 66(3), 217-20.

(16) Xu, C.; Ruan, X. M.; Li, H. Sen; Guo, B. X.; Ren, X. D.; Shuang, J. L.; Zhang, Z. Anti-Adhesive Effect of an Acidic Polysaccharide from Aloe vera L. Var. Chinensis (Haw.) Berger on the Binding of Helicobacter pylori to the MKN-45 Cell Line. J. Pharm. Pharmacol. **2010**, 62 (12), 1753–1759. https://doi.org/10.1111/j.2042-7158.2010.01181.x.

(17) Guzman-Murillo, M.A.; Ascencio F. Anti-adhesive Activity of Sulphated Exopolysaccharides of Microalgae on Attachment of Red Sore Disease-Associated Bacteria and Helicobacter pylori to Tissue Culture Cells. Lett. Appl. Microbiol., **2000,** 30(6), 473-478.

(18) Shibata, H.; Iimuro, M.; Uchiya, N.; Kawamori, T.; Nagaoka, M.; Ueyama, S.; Hashimoto, S.; Yokokura, T.; Sugimura, T.; Wakabayashi, K. Preventive Effects of Cladosiphon Fucoidan against Helicobacter pylori Infection in Mongolian Gerbils. Helicobacter **2003**, 8 (1), 59–65. https://doi.org/10.1046/j.1523-5378.2003.00124.x.19.

(19) Shibata, H.; Kimura-Takagi, I.; Nagaoka, M.; Hashimoto, S.; Sawada, H.; Ueyama, S.; Yokokura, T. Inhibitory Effect of Cladosiphon Fucoidan on the Adhesion of Helicobacter pylori to Human Gastric Cells. J. Nutr. Sci. Vitaminol.. **1999**, 45 (3), 325–336. https://doi.org/10.3177/jnsv.45.325.

(20) Chua, E. G.; Verbrugghe, P.; Perkins, T. T.; Tay, C. Y. Fucoidans Disrupt Adherence of Helicobacter pylori to AGS cells In Vitro. Evid-Based Compl. Alt. **2015.** Article ID 120981. https://doi.org/10.1155/2015/120981

(21) Ascencio, F.; Fransson, L.A.; Wadstrom, T. Affinity of the Gastric Pathogen Helicobacter pylori for the N-Sulfated Glycosaminoglycan Heparan-Sulfate. J. Med. Microbiol. **1993**, 38(4), 240–244.

(22) Icatlo, F. C.; Goshima, H.; Kimura, N.; Kodama, Y. Acid-Dependent Adherence of Helicobacter pylori Urease to Diverse Polysaccharides. Gastroenterology **2000**, 119, 358–367. https://doi.org/10.1053/gast.2000.9372.

(23) Anand, P.; Thomas, S. G.; Kunnumakkara, A. B.; Sundaram, C.; Harikumar, K. B.; Sung, B.; Tharakan, S. T.; Misra, K.; Priyadarsini, I. K.; Rajasekharan, K. N.; Aggarwal, B. B. Biological Activities of Curcumin and its Analogues (Congeners) Made by Man and Mother Nature. Biochem. Pharmacol. **2008**, 76 (11), 1590–1611. https://doi.org/https://doi.org/10.1016/j.bcp.2008.08.008.

(24) Calvo, P.; Remuñán-López, C.; Vila-Jato, J. L.; Alonso, M. J. Development of Positively Charged Colloidal Drug Carriers: Chitosan-Coated Polyester Nanocapsules and Submicron-Emulsions. Colloid Polym. Sci. **1997**, 275 (1), 46–53. https://doi.org/10.1007/s003960050050.

(25) Niehues, M.; Euler, M.; Georgi, G.; Mank, M.; Stahl, B.; Hensel, A. Peptides from Pisum Sativum L. Enzymatic Protein Digest with Anti-Adhesive Activity against Helicobacter pylori: Structure-Activity and Inhibitory Activity against BabA, SabA, HpaA and a Fibronectin-Binding Adhesin. Mol. Nutr. Food Res. **2010**, 54 (12), 1851–1861. https://doi.org/10.1002/mnfr.201000021.

(26) Niehues, M.; Hensel A. In-vitro Interaction of L-dopa with Bacterial Adhesins of Helicobacter pylori: An Explanation for Clinicial Differences in Bioavailability? J. Pharm. Pharmacol. **2009**, 61(10), 1303–1307.

(27) Verheul, R. J.; Amidi, M.; van Steenbergen, M. J.; van Riet, E.; Jiskoot, W.; Hennink, W. E. Influence of the Degree of Acetylation on the Enzymatic Degradation and in Vitro Biological

Properties of Trimethylated Chitosans. Biomaterials **2009**, 30 (18), 3129–3135. https://doi.org/10.1016/j.biomaterials.2009.03.013.
(28) Fessi, H.; Puisieux, F.; Devissaguet, J. P.; Ammoury, N.; Benita, S. Nanocapsule Formation by Interfacial Polymer Deposition Following Solvent Displacement. Int. J. Pharm. **1989**, 55 (1), 1–4. https://doi.org/10.1016/0378-5173(89)90281-0.
(29) Rivera-Rodriguez, G.R.; Alonso, M.J.; Torres, D. Poly-L-Asparagine Nanocapsules as Anticancer Drug Delivery Vehicles. Eur. J. Pharm. Biopharm. **2013**, 85(3), 481–487.
(30) Rosas-Durazo, A.; Lizardi, J.; Higuera-Ciapara, I.; Argüelles-Monal, W.; Goycoolea, F. M. Development and Characterization of Nanocapsules Comprising Dodecyltrimethylammonium Chloride and κ-Carrageenan. Colloid Surfaces B **2011**, 86 (1), 242–246. https://doi.org/10.1016/j.colsurfb.2011.03.020.31.
(31) Oyarzun-Ampuero, F. A.; Rivera-Rodriguez, G. R.; Alonso, M. J.; Torres, D. Hyaluronan Nanocapsules as a New Vehicle for Intracellular Drug Delivery. Eur. J. Pharm. Sci. **2013**, 49 (4), 483–490. https://doi.org/10.1016/j.ejps.2013.05.008.
(32) Guzey, D.; McClements D.J. Formation, Stability and Properties of Multilayer Emulsions for Application in the Food Industry. Adv. Colloid Interfac., **2006**, 128–130, 227–248.
(33) Lertsutthiwong, P., Noomun, K.; Jongaroonngamsang, N.; Rojsitthisak, P.; Nimmannit, U. Preparation of Alginate Nanocapsules Containing Turmeric Oil. Carbohyd. Polym. **2008**, 74 (2), 209–214.
(34) Chen, Y.; Lin, X.; Park, H.; Greever, R. Study of Artemisinin Nanocapsules as Anticancer Drug Delivery Systems. Nanomed.-Nanotechnol. **2009**, 5 (3), 316–322. https://doi.org/10.1016/j.nano.2008.12.005.
(35) Fukui, Y.; Fujimoto, K. The Preparation of Sugar Polymer-Coated Nanocapsules by the Layer-by-Layer Deposition on the Liposome. Langmuir. **2009**. 25 (17), 10020–10025.
(36) Gnanadhas, D. P.; Ben Thomas, M.; Elango, M.; Raichur, A. M.; Chakravortty, D. Chitosan-Dextran Sulphate Nanocapsule Drug Delivery System as an Effective Therapeutic against Intraphagosomal Pathogen Salmonella. J. Antimicrob. Chemother. **2013**, 68 (11), 2576–2586. https://doi.org/10.1093/jac/dkt252.
(37) Haidar, Z.S.; Hamdy, R.C.; Tabrizian, M. Protein Release Kinetics for Core–Shell Hybrid Nanoparticles Based on the Layer-By-Layer Assembly of Alginate and Chitosan on Liposomes. Biomaterials **2008**, 29 (9), 1207–1215.
(38) Pinheiro, A. C.; Bourbon, A. I.; Cerqueira, M. A.; Maricato, É.; Nunes, C.; Coimbra, M. A.; Vicente, A. A. Chitosan/Fucoidan Multilayer Nanocapsules as a Vehicle for Controlled Release of Bioactive Compounds. Carbohydr. Polym. **2015**, 115, 1–9. https://doi.org/10.1016/j.carbpol.2014.07.016.
(39) Preetz, C.; Rübe, A.; Reiche, I.; Hause, G.; Mäder, K. Preparation and Characterization of Biocompatible Oil-Loaded Polyelectrolyte Nanocapsules. Nanomed.-Nanotechnol. **2008**, 4 (2), 106–114. https://doi.org/10.1016/j.nano.2008.03.003.
(40) Kuehner, D. E.; Engmann, J.; Fergg, F.; Wernick, M.; Blanch, H. W.; Prausnitz, J. M. Lysozyme Net Charge and Ion Binding in Concentrated Aqueous Electrolyte Solutions. J. Phys. Chem. B **1999**, 103 (8), 1368–1374. https://doi.org/10.1021/jp983852i.
(41) Blake, C. C. F.; Koenig, D. F.; Mair, G. A.; North, A. C. T.; Phillips, D. C.; Sarma, V. R. Structure of Hen Egg-White Lysozyme - a 3-Dimensional Fourier Synthesis at 2a Resolution. Nature **1965**, 206 (4986), 757–768.
(42) Dickinson, E. Food Emulsions and Foams: Stabilization by Particles. Curr. Opin. Colloid In. **2010**. 15 (1-2), 40–49.
(43) Calvo, P.; Vila Jato, J.L.; Alonso, M. J. Effect of lysozyme on the stability of polyester nanocapsules and nanoparticles: stabilization approaches. Biomaterials **1997**, 18 (19), 1305–1310.
(44) Silletti, E.; Vingerhoeds, M. H.; Norde, W. van Aken, G. The Role of Electrostatics in Saliva-Induced Emulsion Flocculation. Food Hydrocolloid. **2007**, 21 (4), 596–606.

(45) Cao, Y.; Dickinson, E.; Wedlock, D. J. Creaming and Flocculation in Emulsions Containing Polysaccharide. Food Hydrocolloid. **1990**, 4 (3), 185–195.
(46) Quemeneur, F.; Rammal, A.; Rinaudo, M.; Pépin-Donat, B. Large and Giant Vesicles "Decorated" with Chitosan: Effects of PH, Salt or Glucose Stress, and Surface Adhesion. Biomacromolecules **2007**, 8 (8), 2512–2519. https://doi.org/10.1021/bm061227a.
(47) Goycoolea, F. M.; Valle-Gallego, A.; Stefani, R.; Menchicchi, B.; David, L.; Rochas, C.; Santander-Ortega, M. J.; Alonso, M. J. Chitosan-Based Nanocapsules: Physical Characterization, Stability in Biological Media and Capsaicin Encapsulation. Colloid Polym. Sci. **2012**, 290 (14), 1423–1434. https://doi.org/10.1007/s00396-012-2669-z.
(48) Santander-Ortega, M. J.; Peula-García, J. M.; Goycoolea, F. M.; Ortega-Vinuesa, J. L. Chitosan Nanocapsules: Effect of Chitosan Molecular Weight and Acetylation Degree on Electrokinetic Behaviour and Colloidal Stability. Colloids Surfaces B **2011**, 82 (2), 571–580. https://doi.org/10.1016/j.colsurfb.2010.10.019.
(49) Volwerk, J. J.; Jost, P. C.; de Haas, G. H.; Griffith, O. H. Activation of Porcine Pancreatic Phospholipase-A2 by the Presence of Negative Charges at the Lipid Water Interface. Biochemistry **1986**, 25 (7), 1726–1733.
50. Mircheva, K.; Minkov, I.; Ivanova, T.; Panaiotov, I.; Proust, J. E.; Verger, R. Comparative Study of Lipolysis by PLA2 of DOPC Substrates Organized as Monolayers, Bilayer Vesicles and Nanocapsules. Colloids Surfaces B Biointerfaces 2008, 67 (1), 107–114. https://doi.org/10.1016/j.colsurfb.2008.08.007.
Mircheva, K., et al., Comparative study of lipolysis by PLA(2) of DOPC substrates organized as monolayers, bilayer vesicles and nanocapsules. Colloids and Surfaces B-Biointerfaces, 2008. **67**(1): p. 107-114.
51. Jorgensen, K., J. Davidsen, and O.G. Mouritsen, Biophysical mechanisms of phospholipase A2 activation and their use in liposome-based drug delivery. Febs Letters, 2002. **531**(1): p. 23-27.
52. Davidsen, J., et al., Drug delivery by phospholipase A(2) degradable liposomes. International Journal of Pharmaceutics, 2001. **214**(1-2): p. 67-69.
53. Li, Y., et al., Controlling lipid nanoemulsion digestion using nanolaminated biopolymer coatings. Journal of Microencapsulation, 2011. **28**(3): p. 166-175.
54. Cao, A.L., et al., Curcumin induces apoptosis in human gastric carcinoma AGS cells and colon carcinoma HT-29 cells through mitochondrial dysfunction and endoplasmic reticulum stress. Apoptosis, 2013. **18**(11): p. 1391-1402.
55. Raveendran, R., G.S. Bhuvaneshwar, and C.P. Sharma, In vitro cytotoxicity and cellular uptake of curcumin-loaded Pluronic/Polycaprolactone micelles in colorectal adenocarcinoma cells. Journal of Biomaterials Applications, 2013. **27**(7): p. 811-827.
56. Araki, Y., H. Sugihara, and T. Hattori, In vitro effects of dextran sulfate sodium on a Caco-2 cell line and plausible mechanisms for dextran sulfate sodium-induced colitis. Oncology Reports, 2006. **16**(6): p. 1357-1362.
57. Khar, A., et al., Induction of stress response renders human tumor cell lines resistant to curcumin-mediated apoptosis: role of reactive oxygen intermediates. Cell Stress Chaperones, 2001. **6**(4): p. 368-376.
58. Chuah, L.H., et al., Cellular uptake and anticancer effects of mucoadhesive curcumin-containing chitosan nanoparticles. Colloids and Surfaces B: Biointerfaces, 2014. **116**(0): p. 228-236.
59. Zanotto-Filho, A., et al., Curcumin-loaded lipid-core nanocapsules as a strategy to improve pharmacological efficacy of curcumin in glioma treatment. European Journal of Pharmaceutics and Biopharmaceutics, 2013. **83**(2): p. 156-67.
60. Morin, D., et al., Curcumin induces the mitochondrial permeability transition pore mediated by membrane protein thiol oxidation. Febs Letters, 2001. **495**(1-2): p. 131-136.

61. Okayasu I, Hatakeyama S, Yamada M, Ohkusa T, Inagaki Y, Nakaya R. A novel method in the induction of reliable experimental acute and chronic ulcerative colitis in mice. Gastroenterology 1990;98:694-702.
62. Pachekrepapol, U., Horne, D. S., & Lucey, J. A. (2015). Effect of dextran and dextran sulfate on the structural and rheological properties of model acid milk gels. Journal of Dairy Science, 98(5), 2843–2852. https://doi.org/10.3168/jds.2014-8660
63. Kiruthika, V., Maya, S., Suresh, M. K., Anil Kumar, V., Jayakumar, R., & Biswas, R. (2015). Comparative efficacy of chloramphenicol loaded chondroitin sulfate and dextran sulfate nanoparticles to treat intracellular Salmonella infections. Colloids and Surfaces B: Biointerfaces, 127, 33–40. https://doi.org/10.1016/j.colsurfb.2015.01.012
64. Goncalves, I.C., et al., Bacterial-binding chitosan microspheres for gastric infection treatment and prevention. Acta Biomaterialia, 2013. **9**(12): p. 9370-8.
65. Parreira, P., et al., Effect of surface chemistry on bacterial adhesion, viability, and morphology. J Biomed Mater Res A, 2011. **99**(3): p. 344-53.
66. Qin, X., et al., An investigation of the interactions between an E. coli bacterial quorum sensing biosensor and chitosan-based nanocapsules. Colloids Surf B Biointerfaces, 2017. **149**: p. 358-368.
67. Larsen, M.U., et al., Biocompatible Nanoparticles Trigger Rapid Bacteria Clustering. Biotechnology Progress, 2009. **25**(4): p. 1094-1102.
68. Rafsanjany, N., et al., Antiadhesion as a functional concept for protection against uropathogenic Escherichia coli: In vitro studies with traditionally used plants with antiadhesive activity against uropathognic Escherichia coli. Journal of Ethnopharmacology, 2013. **145**(2): p. 591-597.
69. Nogueira, F., I.C. Goncalves, and M.C.L. Martins, Effect of gastric environment on Helicobacter pylori adhesion to a mucoadhesive polymer. Acta Biomaterialia, 2013. **9**(2): p. 5208-5215.
70. Jain, P., et al., Polyelectrolyte coated multilayered liposomes (nanocapsules) for the treatment of Helicobacter pylori infection. Mol Pharm, 2009. **6**(2): p. 593-603.
71. Utt, M. and T. Wadstrom, Identification of heparan sulphate binding surface proteins of Helicobacter pylori: Inhibition of heparan sulphate binding with sulphated carbohydrate polymers. Journal of Medical Microbiology, 1997. **46**(7): p. 541-546.
72. Van de Bovenkamp JH, Mahdavi J, Korteland-Van Male AM, Buller HA, Einerhand AW, Boren T, et al. The MUC5AC glycoprotein is the primary receptor for Helicobacter pylori in the human stomach. Helicobacter. 2003; 8(5): 521-32